ACS Photonics

pubs.acs.org/journal/apchd5

Article

Lighting Up Si Nanoparticle Arrays by Exploiting the Bound States in the Continuum Formed in a Si/Au Hybrid Nanostructure

Lidan Zhou,[#] Mingcheng Panmai,[#] Shulei Li, Yuheng Mao, Weichen He, Hongxin Huang, and Sheng Lan*

Cite This: *ACS Photonics* 2022, 9, 2991−2999

Read Online

ACCESS | Metrics & More | Article Recommendations | Supporting Information

ABSTRACT: Silicon (Si)-based light emitters compatible with the current fabrication technology of Si chips are crucial for realizing all-optical computation. Here, we propose a Si/Au hybrid nanostructure composed of a regular array of Si nanopillars and a thin gold (Au) film. An accidental bound state in the continuum (BIC) originating from the interference of the mirror-image-induced magnetic dipole and the surface plasmon polariton can be achieved in the nanostructure by deliberately designing the structure parameters. Efficient nonlinear optical emission is observed when the nanostructure is excited by using femtosecond laser pulses. The lowest threshold for the burst of luminescence from the Si nanoparticle is observed at the BIC, where the nonlinear optical absorption is greatly enhanced. It is found that the excitation of the surface plasmon polariton is crucial for taking the advantage of the BIC, which is manifested in the low threshold and special radiation pattern. Our findings open new horizons for manipulating light-matter interaction by exploiting the BICs created in dielectric-metal hybrid nanostructures.

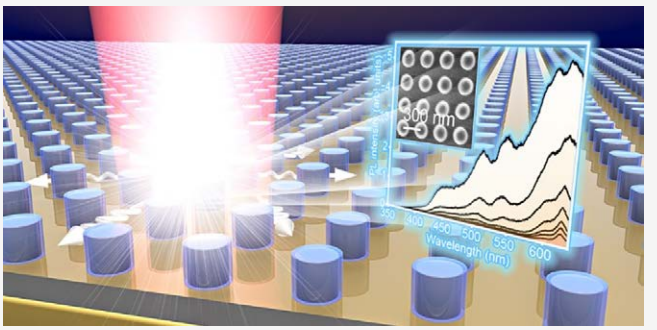

KEYWORDS: *Si/Au hybrid nanostructure, bound state in the continuum, surface plasmon polariton, nonlinear optical absorption, hot electron luminescence*

INTRODUCTION

Semiconductors are generally classified into two types with direct and indirect bandgap structures, which are clearly distinct in the absorption and emission of photons. As a semiconductor with indirect bandgap, silicon (Si) in the bulk form exhibits a quantum efficiency as low as $\sim 10^{-7}$ and is considered as a poor photon emitter.[1] How to improve the quantum efficiency of Si has been a long-standing challenge faced by scientists. So far, the strategies for enhancing the quantum efficiency of Si focus mainly on the engineering of its band structure, such as making porous Si,[2,3] Si quantum dots,[4−7] and Si/Ge alloy.[8,9] Although this idea has been demonstrated to be successful, the light sources based on porous Si or Si quantum dots[10,11] are incompatible with the current fabrication technology of Si chips, which severely hinders their application in integrated optical circuits.

Apart from band structure engineering, an alternative for improving the quantum efficiency of Si, which has long been overlooked, relies on the enhancement of light-matter interaction.[12] In principle, optical cavities with high quality factors and small mode volumes are highly desirable for enhancing light-matter interaction.[13−15] From the viewpoint of practical applications, however, spectrum[16] and mode[17] matching between the excitation light and the optical cavity are more important for achieving this goal when ultrashort pulse or structured light is employed as the excitation source. In recent years, much effort has been devoted to dielectric nanoparticles[18] with large refractive indices because they are considered as the building blocks for metamaterials operating at optical frequencies.[19−21] A typical example is Si nanoparticles with diameters of 150−250 nm, which support electric dipole (ED)[22] and magnetic dipole (MD)[23] resonances in the visible and near-infrared spectral range.[24−27] Although the quality factors of these resonances are not large, it has been demonstrated that Si nanoparticles can be lighten up by resonantly exciting their ED/MD resonances, leading to a quantum efficiency of ∼1.0%.[28] In this case, the enhancement in the quantum efficiency by nearly 5 orders of magnitude is achieved by modifying the carrier dynamics in Si nanoparticles through injecting dense electron−hole plasma.[29] The Auger effect, which is proportional to the cubic of the carrier density, plays a crucial role in this scenario.[30] By placing Si nanoparticles on a thin metal film, it

Received: April 25, 2022
Published: August 16, 2022

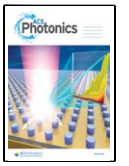

https://doi.org/10.1021/acsphotonics.2c00618
ACS Photonics 2022, 9, 2991−2999

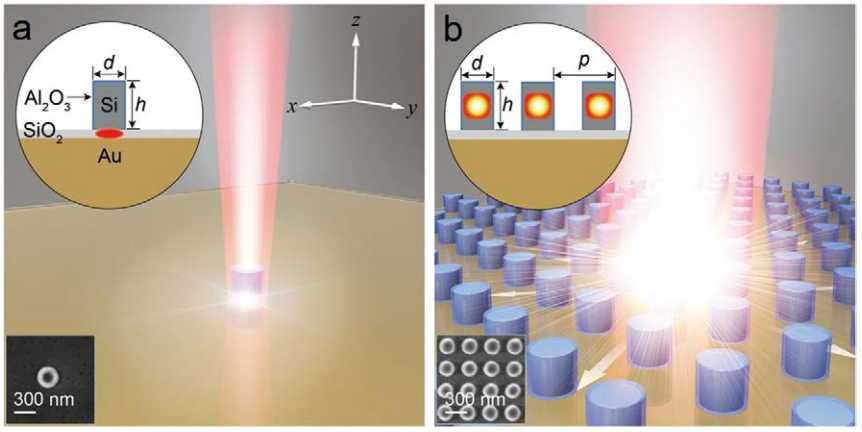

Figure 1. Configurations of Si/Au hybrid nanostructures supporting MMD and BIC. Schematic showing the configurations for the regular arrays of (a) isolated and (b) coupled Si nanopillars fabricated on Au/SiO_2 substrates and the hot electron luminescence emitted from Si nanopillars under the excitation of femtosecond laser pulses. The detailed sample structures (including geometrical parameters) and the SEM images of the fabricated Si nanopillars are shown in the insets. Here, we use *d*, *h*, and *p* to represent the diameter and height of Si nanopillars and the period of the square lattice of Si nanopillars, respectively.

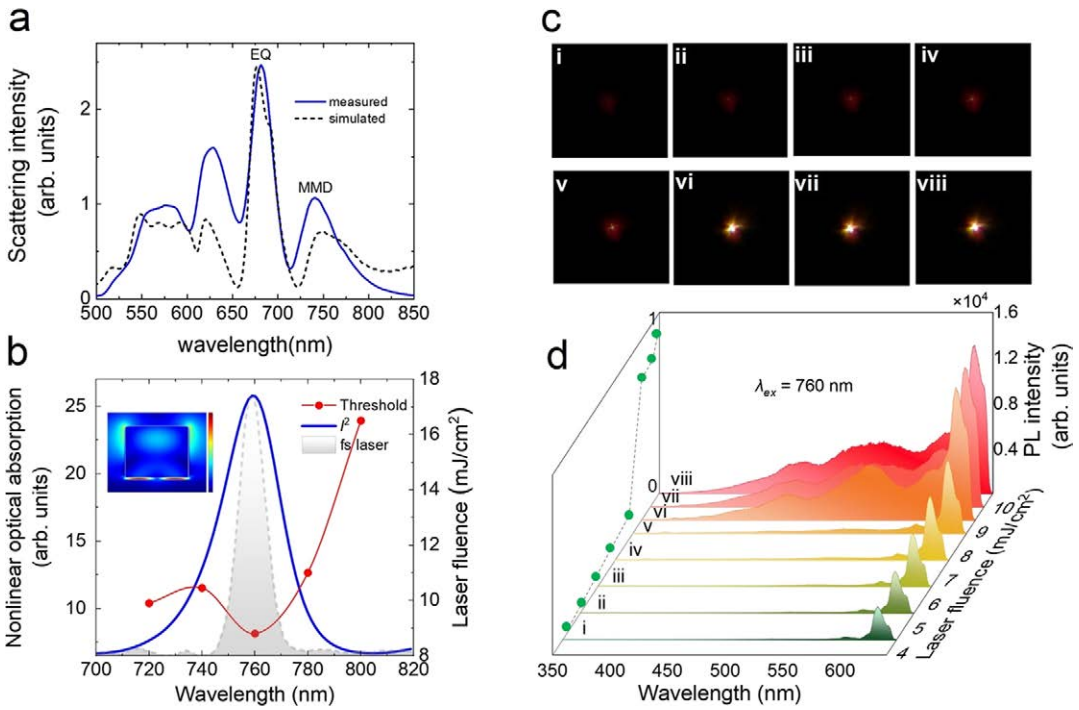

Figure 2. Nonlinear optical emission from Si nanopillars mediated by MMD. (a) Backward scattering spectra calculated (dashed curve) and measured (solid curve) for an isolated Si nanopillar (h = 220 nm, d = 260 nm) on a Au/SiO_2 substrate. (b) 2PA spectrum (or I^2 spectrum) calculated for a Si nanopillar (h = 220 nm, d = 260 nm) on a Au/SiO_2 substrate. The electric field distribution in the *X*-*Z* plane is shown in the inset. (c) CCD images of the hot electron luminescence from the Si nanopillar recorded at different excitation irradiances. (d) Evolution of the luminescence spectrum of the Si nanopillar with increasing excitation irradiance. The excitation wavelength was chosen to be λ_{ex} = 760 nm.

was demonstrated very recently that the quantum efficiency can be further improved to ~6.0−8.0%[31] by exploiting the strongly localized electric field and dramatically reduced linewidth provided by the so-called mirror-image-induced magnetic dipole (MMD) resonance.[32,33] In addition, the good thermal conductivity of the metal film enables the stable emission of white light for a long time. It was shown that surface lattice resonances with quality factors larger than those of the MMD resonance can be achieved in a regular array of Si nanopillars, which offers a larger nonlinear optical absorption.[31] However, the quality factors of surface lattice resonances are still too small to match the linewidth of the femtosecond laser pulses, implying the existence of more space for boosting light-matter interaction via creating optical resonances with larger quality factors.

In recent years, bound states in the continuum (BICs)[34−36] have attracted great interest owing to the infinitely large quality factors theoretically predicted for these optical resonances.[37] Basically, BICs can be classified into symmetry-protected BICs and accidental (Friedrich−Wintgen or FW) BICs.[38,39] While the former originates from the mismatch in symmetry between the optical mode and the incident wave, the latter arises from the interference of two optical modes.[40] So far, both BICs have been exploited to enhance light-matter interaction, such as the

https://doi.org/10.1021/acsphotonics.2c00618
ACS Photonics 2022, 9, 2991−2999

realization of lasers[41,42] and achievement of highly efficient harmonic generation.[43,44] In most cases, all-dielectric nanostructures with extremely low optical losses are employed because the high quality factors of BICs are generally pursued.[45−47] In comparison, less attention has been paid to dielectric-metal hybrid nanostructures owing to the Ohmic loss of metals, which may influence the quality factors of BICs.[33,48] Recent studies reveal that two types of BICs with quality factors as large as ∼800 can also be realized in dielectric-metal hybrid nanostructures by exploiting the surface plasmon polaritons (SPPs) generated on the surfaces of metal films.[49] Considering the spectrum match between the optical mode and the excitation light (e.g., femtosecond laser pulses), BICs with quality factors of ∼100 are sufficient to dramatically enhance the nonlinear optical absorption of Si nanoparticles.[50]

In this article, we proposed a dielectric-metal hybrid nanostructure, which is composed of a regular array of Si nanopillars and a thin gold (Au) film, to create an accidental BIC with a moderate quality factor. We revealed that the BIC originates from the interference between the MMD and SPP modes. We found that the electric field at the BIC is strongly localized in Si nanoparticles, leading to a dramatic increase in the nonlinear optical absorption of Si nanoparticles. We demonstrated that the minimum threshold for the luminescence burst is obtained at the BIC, which is about 1 order of magnitude smaller than that observed at the MMD of single Si nanoparticles. We showed that the efficient excitation of the SPPs is crucial for fully exploiting the enhanced nonlinear optical absorption at the BIC.

RESULTS AND DISCUSSION

In Figure 1, we show schematically regular arrays of isolated and coupled Si nanopillars with a diameter of d and a height of h, which correspond to Si nanopillars without and with interaction, fabricated on SiO_2/Au/Si substrates. The pitches (p) for the regular arrays of isolated and coupled Si nanopillars were designed to be p = 5.0 μm and p = 320 nm, respectively. The detailed configurations of such dielectric−metal hybrid nanostructures are depicted in the insets. Si nanopillars were separated from the Au film by using a 10 nm-thick SiO_2 layer. In addition, they were covered with a 5 nm-thick Al_2O_3 layer, which was used to eliminate the nonradiative recombination centers induced in the fabrication process (see the Methods section for the details). The scanning electron microscopy (SEM) images of the isolated and coupled Si nanopillars are also provided as insets (see the Supporting Information, Figure S1).

In Figure 2a, we present the backward scattering spectrum simulated for an isolated Si nanopillar (d = 260 nm, h = 220 nm) located on a SiO_2/Au/Si substrate. The thin SiO_2 spacer layer (t_{SiO2} = 10 nm) and the thin Al_2O_3 passivation layer (t_{Al2O3} = 5 nm) were taken into account. In the scattering spectrum, one can identify several optical resonances in the visible to infrared spectral range, as marked by color arrows. Here, we focus mainly on the optical resonance at λ ∼760 nm, which can be easily accessed by using conventional femtosecond laser light. Based on previous studies, this optical resonance is attributed to the MMD originating from the interference between the ED excited in the Si nanopillar and its mirror image induced by the Au film.[32,49] We also performed a multipolar expansion analysis for the backward scattering spectrum of the Si nanopillar and identified the physical origins for the optical resonances appearing in the scattering spectrum (see the Supporting Information, Figure S2). In Figure 2a, we also provide the backward scattering spectrum measured for a Si nanopillar with d = 260 nm. Except the relative intensities among the optical resonances, the experimental observation is in good agreement with the simulation result. The discrepancy between the simulated and measured scattering spectra may be caused by the incident angle of the illumination light. As demonstrated before, the optical resonances supported by a Si nanoparticle can be employed to enhance the nonlinear optical absorption of the Si nanoparticle, which can be evaluated by using the integration of $|E|^4$ over the volume of the Si nanopillar,[28,31] as shown in Figure 2b. Specifically, the electric field distribution in the X-Z plane calculated at the MMD (λ = 760 nm) is shown in the inset. It is noticed that the electric field is strongly localized in the SiO_2 spacer layer between the Si nanopillar and the Au film. As a result, the electric field inside the Si nanopillar is also enhanced to some extent, leading to the enhancement in the nonlinear optical absorption.

In experiments, we excited isolated Si nanopillars by using femtosecond laser pulses in the wavelength range of 720−800 nm. The femtosecond laser light was focused on Si nanopillars by using a 60× objective with NA = 0.85. The diameter of the laser spot was estimated to be ϕ ∼1.36 μm. In all cases, we observed the burst of the hot electron luminescence from Si nanoparticles when the laser fluence (or excitation irradiance) exceeds a threshold. The images of the emitted luminescence recorded by using a charge coupled device (CCD) at different excitation irradiances are shown in Figure 2c. In Figure 2d, we show the evolution of the luminescence spectrum with increasing excitation irradiance for the laser wavelength of λ_{ex} = 760 nm. To the best of our knowledge, this is the first demonstration of the luminescence burst from a single Si nanopillar fabricated by using the current fabrication technology of Si chips. In Figure 2b, we summarize the thresholds for the luminescence burst observed at different excitation wavelengths. It is remarkable that the lowest threshold is achieved at λ_{ex} = 760 nm, where the largest nonlinear optical absorption is expected.

For an isolated Si nanopillar, the quality factor of the MMD is only ∼10 (see Figure 2a) and the electric field is mainly localized in the gap region between the Si nanopillar and the Au film (see the inset of Figure 2b). These two features strongly limit the nonlinear optical absorption of the Si nanopillar. If we compare the linewidth of the nonlinear optical absorption with that of the femtosecond laser pulses (see Figure 2b), the latter is much narrower than the former. It implies that the nonlinear optical absorption of Si nanopillars can be further improved by designing optical resonances with higher quality factors. Fortunately, the recent studies indicate that BICs or quasi-BICs are promising candidates for achieving this goal.

By reducing the pitch of the regular array to p = 320 nm, the momentum conservation conditions necessary for exciting the SPP on the surface of the Au film can be fulfilled. In this case, the regular array of Si nanopillars acts as a nanograting, which couples the incident wave into the SPP propagating on the surface of the Au film. By properly designing the geometrical parameters (see the Supporting Information, Figure S3), the interference between the MMD and SPP modes may lead to the formation of an accidental BIC. As a result, one can expect a quality factor much larger than that of the MMD as well as an electric field strongly localized in Si nanopillars. The

https://doi.org/10.1021/acsphotonics.2c00618
ACS Photonics 2022, 9, 2991−2999

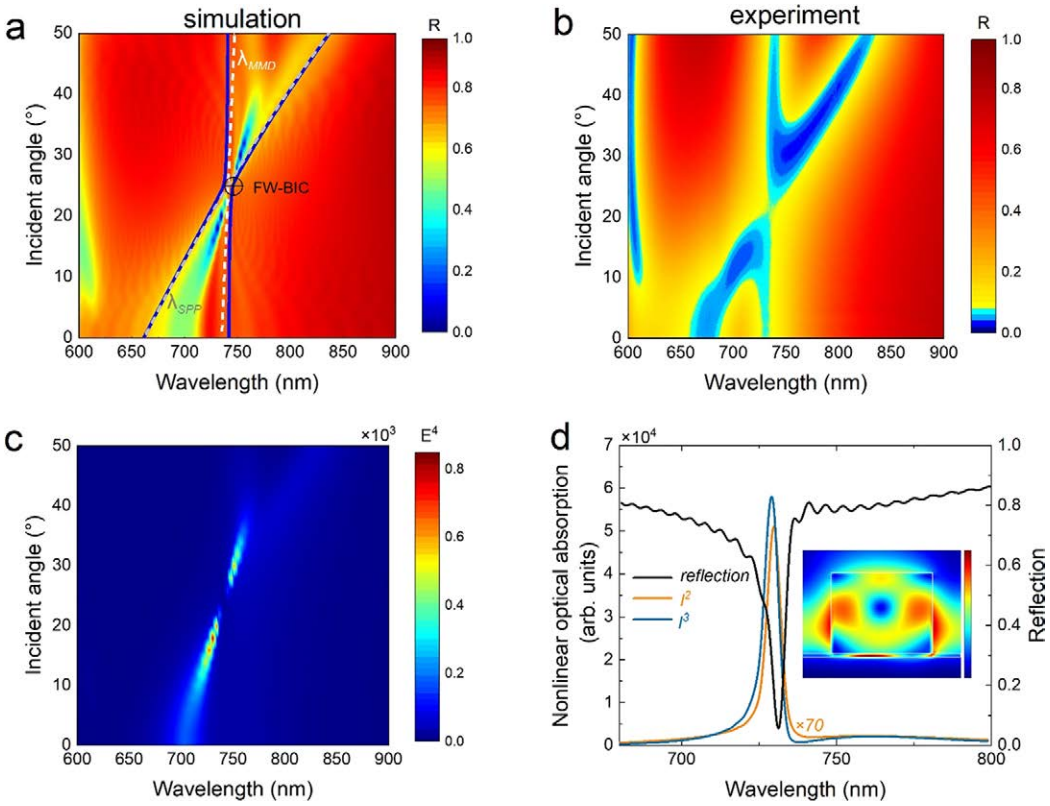

Figure 3. Linear and nonlinear optical properties of the Si/Au hybrid nanostructure supporting BIC. Two-dimensional reflection spectra calculated (a) and measured (b) for the regular array of Si nanopillars (h = 220 nm, d = 190 nm, p = 320 nm) at different incident angles. (c) Two-dimensional 2PA spectra (or I^2 spectra) calculated for the regular array of Si nanopillars at different incident angles. (d) 2PA and 3PA spectra (or I^2 and I^3 spectra) calculated for a Si nanopillar in the regular array of at an incident angle of θ = 21°. The reflection spectrum obtained at the same incident angle is also provided for reference. The electric field distribution in the X-Z plane is shown in the inset.

combination of these two features leads to a significantly enhanced nonlinear optical absorption for Si nanopillars.

In Figure 3a, we present the angle-resolved reflection spectra calculated for a regular array of Si nanopillars with p = 320 nm. For normally incident light (θ = 0°), two reflection dips, which correspond to the SPP and MMD modes, are observed at ∼660 and ∼740 nm. With increasing incident angle, a redshift of the SPP is observed. In comparison, the MMD remains nearly unchanged. As a result, the SPP will intersect with the MMD at an incident angle of θ ∼22°, leading to an anti-crossing region in which the accidental BIC is created. In this case, the BIC is expected to appear at ∼740 nm.

Basically, the BIC formed by the interaction between the SPP and the MMD belongs to FW-BIC, which can be analyzed by using the temporal coupled-mode theory.[51,52] Assuming that the two modes are coupled through the same radiation channel, the Hamiltonian describing the interaction between them can be written as follows:

$$H = \begin{bmatrix} \omega_{SPP} & \kappa \\ \kappa & \omega_{MMD} \end{bmatrix} - i \begin{bmatrix} \gamma_{SPP} & \sqrt{\gamma_{SPP}\gamma_{MMD}}\exp(i\psi) \\ \sqrt{\gamma_{SPP}\gamma_{MMD}}\exp(-i\psi) & \gamma_{MMD} \end{bmatrix} \quad (1)$$

Here, ω_{SPP} and ω_{MMD} represent the resonant frequencies of the SPP and MMD modes, respectively, γ_{SPP} and γ_{MMD} denote the corresponding decay rates, κ and $\sqrt{\gamma_{SPP}\gamma_{MMD}}\exp(\pm i\psi)$ characterize the near-field and radiation coupling, respectively, and Ψ is the phase shift of radiation interference between the two modes, which can be made to be 0 or π through parameter tuning or forced by symmetry. In this way, the resonant frequencies of the two hybrid states are expressed as follows:

$$\omega_{\pm} = \frac{\omega_{SPP} + \omega_{MMD}}{2} - i\frac{\gamma_{SPP} + \gamma_{MMD}}{2} \pm \frac{1}{2}\left([(\omega_{SPP} - \omega_{MMD})] - i(\gamma_{SPP} - \gamma_{MMD})\right)^2 + 4(\kappa - i\sqrt{\gamma_{SPP}\gamma_{MMD}}\exp(i\psi)^2)^{1/2} \quad (2)$$

Considering a specific condition (i.e., the BIC condition) given in the following:

$$\kappa(\gamma_{SPP} - \gamma_{MMD})e^{-i\psi} = \sqrt{\gamma_{SPP}\gamma_{MMD}}(\omega_{SPP} - \omega_{MMD}) \quad (3)$$

When such a condition is fulfilled, the resonant frequencies of the two hybrid states can be simplified as

$$\omega_{+} = \frac{\omega_{SPP} + \omega_{MMD}}{2} + \frac{\kappa(\gamma_{SPP} + \gamma_{MMD})}{2\sqrt{\gamma_{SPP}\gamma_{MMD}}e^{i\psi}} - i(\gamma_{SPP} + \gamma_{MMD}) \quad (4)$$

$$\omega_{-} = \frac{\omega_{SPP} + \omega_{MMD}}{2} - \frac{\kappa(\gamma_{SPP} + \gamma_{MMD})}{2\sqrt{\gamma_{SPP}\gamma_{MMD}}e^{i\psi}} \quad (5)$$

Near the anti-crossing point, it is noticed that one hybrid state (ω_{+}) becomes more lossy (with an imaginary part of γ_{SPP} + γ_{MMD}) while the other (ω_{-}) becomes lossless (without an imaginary part or with an infinite Q factor). In this case, the FW-BIC appears in the lower hybrid state.

We fitted the angle-resolved reflection spectrum shown in Figure 3a with the theoretical mode based on the temporal

https://doi.org/10.1021/acsphotonics.2c00618
ACS Photonics 2022, 9, 2991−2999

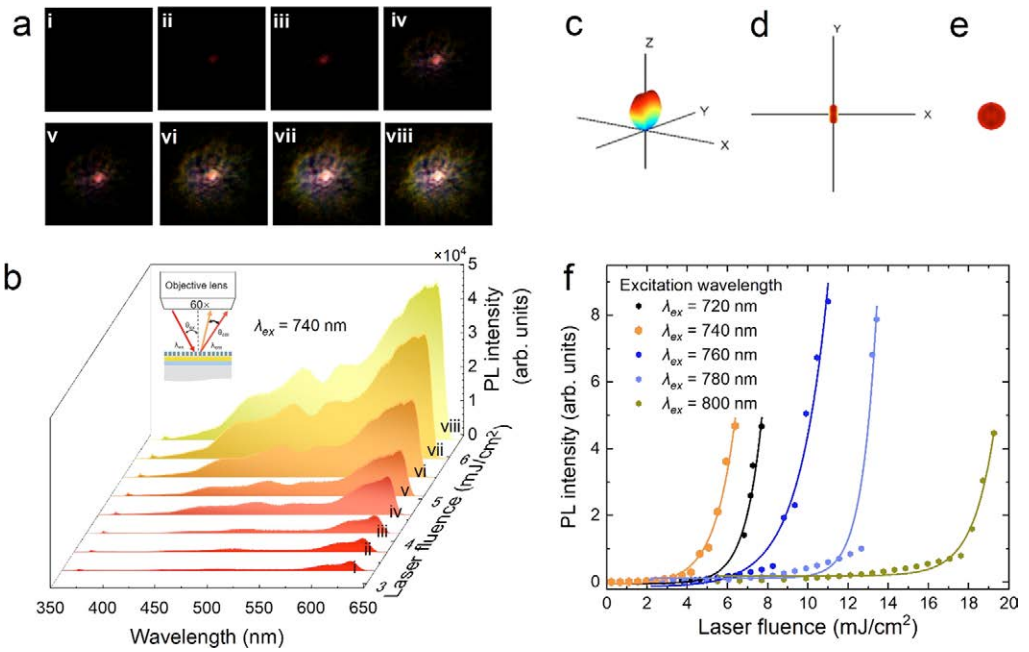

Figure 4. Nonlinear optical emission from Si nanopillars excited by using an objective with a large NA. (a) CCD images of the hot electron luminescence from the Si nanopillars recorded at different excitation irradiances (left panel). (b) Evolution of the luminescence spectrum of the regular array of Si nanopillars (h = 220 nm, d = 190 nm, p = 320 nm) with increasing excitation irradiance. The femtosecond laser light was focused on Si nanopillars by using a 60× objective. The excitation wavelength was chosen to be λ_{ex} = 740 nm. (c−e) 3D radiation patterns calculated for the regular array of Si nanopillars, which is excited by using a dipole source placed in the central Si nanopillar and oriented in the x direction. The top view radiation pattern derived for randomly distributed dipole sources is also presented. (f) Dependences of the luminescence intensity on the excitation irradiance obtained at different excitation wavelengths. In each case, the experimental data is fitted by an exponential rise function.

coupled-mode theory described above. The parameters used in the fitting are κ = 0.012 meV, γ_{SPP} = 0.068 meV, and γ_{MMD} = 0.032 meV (see the Supporting Information, Figure S4).

In Figure 3b, we show the angle-resolved reflection spectra measured for a regular array of Si nanopillars with d = 190 nm and p = 320 nm. It is found that the measured reflection spectra are in excellent agreement with the simulated ones (see Figures S5 and S6). To gain a deep insight into the enhancement of the nonlinear optical absorption at the BIC, we calculated the angle-resolved nonlinear optical absorption spectra, which are characterized by $I^2 = (\int |E|^4 dV)/V$ for two-photon-induced absorption (2PA), for a Si nanopillar in the array, as shown in Figure 3c. It is remarkable that the largest 2PA is indeed achieved around the BIC, which appears at λ ~740 nm and θ ~22°. The reduction of the 2PA at the BIC is caused mainly by the difficulty in coupling the incident plane wave into the BIC. In Figure 3d, we show the 2PA spectrum calculated at θ = 21°, which is close to the BIC. The corresponding reflection spectrum is also provided for reference. In this case, the quality factor of the optical mode in the reflection spectrum is estimated to be ~150, which is much larger than that observed at the MMD (see Figure 2b). Accordingly, the nonlinear optical absorptions originating from 2PA and three-photon-induced absorption (3PA) are dramatically enhanced by factors of ~700 and ~60,000, respectively. More importantly, it is found that the electric field is mainly localized inside the Si nanopillar (see the inset of Figure 3d). This unique feature is responsible for the significant enhancement in the nonlinear optical absorption of the Si nanopillar.

To confirm the above prediction, we excited a regular array of Si nanopillars by using femtosecond laser pulses with different wavelengths ranging from 720 to 800 nm. Similarly, the femtosecond laser light was focused on Si nanopillars by using a 60× objective. Since 2PA and 3PA are expected to be dependent on I^2 and I^3, it is estimated that only a few Si nanopillars around the laser spot center are effectively excited. In each case, we observed the luminescence burst above a threshold, as evidenced in Figure 4a where the CCD images of the hot electron luminescence from Si nanopillars are presented. As an example, we show the evolution of the luminescence spectrum with increasing laser fluence for λ_{ex} = 740 nm (see Figure 4b). In Figure 4c−e, we present the three-dimensional (3D) radiation pattern simulated for a 3 × 3 regular array of Si nanopillars at an emission wavelength of λ_{em} = 555 nm. To mimic the excitation of the array by using a 60× objective, we placed a dipole source oriented in the x direction only in the central Si nanopillar. The other Si nanopillars act only as scatters of the emitting light. One can find an elongated radiation along the y direction (see Figure 4d). Assuming that the dipole sources are randomly oriented, the top view of the radiation pattern will appear as a small bright spot, as shown in Figure 4e. We examined the luminescence burst behaviors at different excitation wavelengths, as shown in Figure 4f. In each case, the luminescence intensity increases exponentially with increasing laser fluence above the threshold. As expected, the lowest threshold was found at the BIC (λ ~740 nm). It is noticed, however, that the threshold for the regular array of Si nanopillars was reduced only by a factor of ~1.6 as compared with isolated Si nanopillars, implying that the nonlinear optical absorption is not greatly enhanced in the case. Owing to the relatively large numerical aperture (NA) of the objective, the number of Si nanopillars covered by the laser spot is quite small and the SPP is not effectively excited. It is noticed that the luminescence emitted from the regular array of the Si nanopillar exhibits a color similar to that emitted from a single nanopillar (see Figures 2a and 4c). In addition, it was found

https://doi.org/10.1021/acsphotonics.2c00618
ACS Photonics 2022, 9, 2991−2999

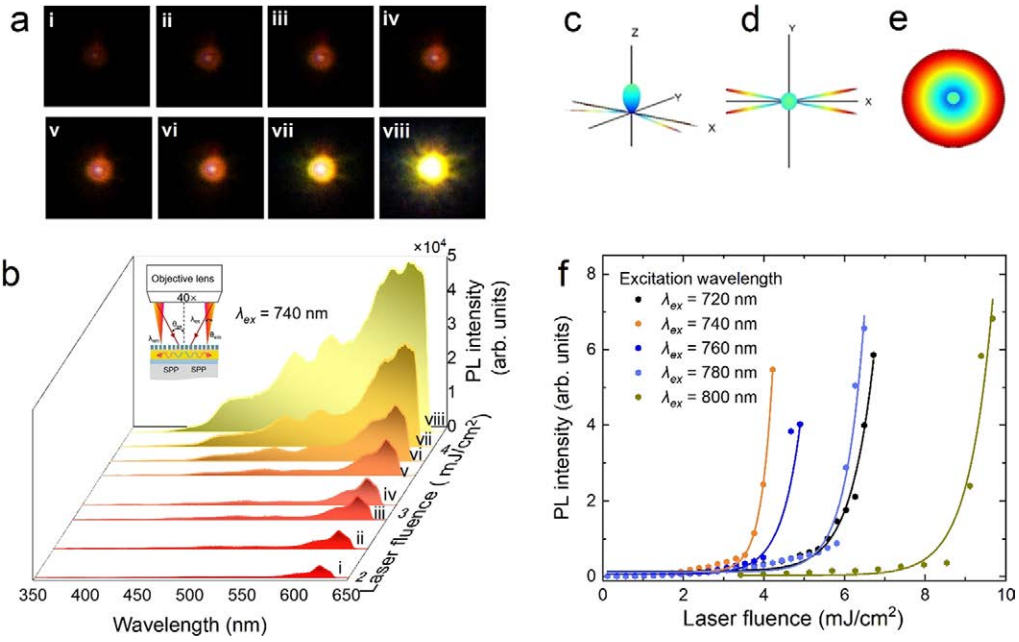

Figure 5. Nonlinear optical emission from Si nanopillars excited by using an objective with a small NA. (a) CCD images of the hot electron luminescence from the Si nanopillars recorded at different excitation irradiances. (b) Evolution of the luminescence spectrum of the regular array of Si nanopillars (h = 220 nm, d = 190 nm, p = 320 nm) with increasing excitation irradiance. The femtosecond laser light was focused on Si nanopillars by using a 40× objective. The excitation wavelength was chosen to be λ_{ex} = 740 nm. (c−e) 3D radiation patterns calculated for the 3 × 3 regular array of Si nanopillars, which are excited by using in-phase dipole sources oriented in the x direction, are also provided. The top view radiation pattern derived for randomly distributed dipole sources is also presented. (f) Dependences of the luminescence intensity on the excitation irradiance obtained at different excitation wavelengths. In each case, the experimental data is fitted by an exponential rise function.

that the luminescence emitted from the central Si nanopillar of the array is scattered by the neighboring Si nanopillars (see Figure 4a).

To verify this suspect, we replaced the 60× objective with a 40× objective (NA = 0.60), which possesses a larger laser spot diameter of ϕ ∼1.88 μm. In this case, it was estimated that more than 3 × 3 Si nanopillars will be effectively excited. Similarly, we observed luminescence burst in all cases and found the lowest threshold at the BIC (∼740 nm), as shown in Figure 5a. It is remarkable that the radiation pattern of the luminescence is much different from that observed in Figure 4a, where a 60× objective was employed. At low laser fluences, the radiation pattern is composed of a central bright spot surrounded by a bright ring. It becomes a bright spot with a large diameter at high laser fluences. The evolution of the luminescence spectrum with increasing laser fluence measured at the BIC (λ_{ex} = 740 nm) is presented in Figure 5b. In this case, the SPPs propagating on the surface of the Au film will be excited by the oblique incident excitation laser light (λ_{ex}) with the help of the nanograting composed of Si nanopillars, as schematically shown in the inset. As a result, the number of Si nanopillars being excited by the laser light is much larger than that covered by the laser spot. In addition, the nonlinear optical emission in the visible light spectrum will emit into free space with the help of the same nanograting. The luminescence with a certain wavelength (λ_{em}) will emit at a specified angle (θ_{em}). Since the luminescence band is narrow at low laser fluences, the emission pattern originating from the Si nanopillars excited by the SPPs appears as a ring because of the fixed emission angle (θ_{em}). At high laser fluences, the luminescence band becomes very broad and the emission pattern appears to be a spot with a diameter as large as ∼12 μm. We simulated the radiation pattern of a 3 × 3 array of Si nanopillars by placing in-phase x-oriented dipoles in all Si nanopillars. The simulation results for an emission wavelength of λ_{em} = 555 nm are presented in Figure 5c−e. Similarly, the radiation pattern in the X-Y plane resulting from randomly oriented dipole sources in all Si nanopillars (see Figure 5e) was obtained by rotating the radiation pattern of an x-oriented dipole source (see Figure 5d). It is in good agreement with the experimental observation (see Figure 5a), implying that the luminescence obtained in this case originates from the coherent radiation of many Si nanopillars. In Figure 5f, we present the dependence of the luminescence intensity on the laser fluence obtained at different excitation wavelengths. Similarly, an exponential increase in the luminescence intensity with increasing laser fluence is observed in each case above the threshold. Surprisingly, it was found that the threshold at each laser wavelength was smaller than that observed by using the 60× objective (see Figure 4f). Accordingly, the luminescence intensity above the threshold was greatly enhanced based on the CCD images. Therefore, it was confirmed that the excitation of the SPP is crucial for the formation of the BIC where the nonlinear optical absorption of Si nanopillars can be significantly enhanced.

CONCLUSIONS

In summary, we have proposed a dielectric-metal hybrid nanostructure composed of a regular array of Si nanopillars and a thin Au film and demonstrated the formation of accident BIC by appropriately designing the structural parameters. As compared with the MMD created for isolated Si nanopillars placed on the Au film, a significant enhancement in both the quality factor and the nonlinear optical absorption is observed at the BIC, leading to a dramatic reduction in the threshold for the luminescence burst. It is revealed that the effective

https://doi.org/10.1021/acsphotonics.2c00618
ACS Photonics 2022, 9, 2991−2999

excitation of the SPP mode is crucial for fully exploiting the BIC-enhanced nonlinear optical absorption, which can be realized by using an objective with a small NA. Our findings open new horizons for enhancing light-matter interaction by exploiting the BICs formed in dielectric-metal hybrid nanostructures and pave the way for realizing efficient light sources based on crystalline Si nanoparticles fabricated by using the current fabrication technology of Si chips.

METHODS

Sample Fabrication. In this work, we transferred the thin crystalline-silicon (c-Si) film of a silicon-on-insulator (SOI) wafer to a quartz substrate by using the combination of adhesive wafer bonding and chemical polishing (see the Supporting Information, Figure S7). First, a 100 nm-thick gold (Au) film and a 10 nm-thick silica (SiO_2) film were deposited sequentially on a SOI wafer comprising a 220 nm-thick c-Si film on a 2 μm-thick SiO_2 substrate. Then, a ultraviolet light curable adhesive (NOA61) was spin-coated on the sample followed by bonding to the quartz substrate. After that, the sample was illuminated by using 365 nm ultraviolet LED light to cross-link the adhesive for 4 h. To achieve optimum adhesion, the sample was beforehand baked at 50 °C for 1 day. The Si substrate was then removed by chemical polishing and dry etching. Finally, the c-Si on the quartz substrate was obtained by removing the SiO_2 substrate of the SOI wafer with hydrofluoric (HF) acid.

Patterning of Si nanopillars was realized by using the combination of electron-beam exposure of positive resist and dry etching. The sample was first spin-coated with 400 nm-thick resist for the electron beam (ARP6200.09). Then, the pattern was exposed by using an electron-beam lithography system (EBPG5000Plus, Raith) operated at 100 kV. After that, the resist was developed with xylene and the pattern transfer was realized by using an inductively coupled plasma tool (Oxford Instruments). To eliminate the nonradiative recombination centers induced in the fabrication process, the fabricated Si nanopillars were covered with a 5 nm-thick Al_2O_3 layer by using an atomic layer deposition system (SUNALE R-150, Picosun). The procedure for fabricating regular arrays of Si nanopillars is described in detail in Note S5. The morphology of Si nanopillars was characterized by using scanning electron microscopy (Auriga, Zeiss), as shown in Figures S1 and S8.

Optical Characterization. The linear and nonlinear optical properties of Si/Au hybrid nanostructures were characterized by using an inverted microscope (Observer A1, Zeiss) equipped with white light and femtosecond laser light as excitation sources (see the Supporting Information, Figure S9).

The scattering spectra of isolated Si nanopillars were measured by using a dark-field microscope. In this case, the illumination light was incident on Si nanopillars at an angle of ~40° and the forward/backward scattering light was collected by the objective of a dark-field microscope. The angled-resolved reflection spectra of the regular arrays of Si nanopillars were measured by using a commercially available optical system (ARM, Ideaoptics).

For nonlinear optical responses, we used femtosecond laser pulses with a duration of 130 fs and a repetition rate of 76 MHz (Mira 900S, Coherent) to excite Si nanopillars. The excitation light was focused on Si nanopillars by using a 60× or a 40× objective of the microscope, and the hot electron luminescence emitted from Si nanopillars was collected by using the same objective and directed to a spectrometer (SR-500i-B1, Andor) for spectral analysis or to a charge-coupled device (DU970N, Andor) for imaging.

Numerical Simulation. The reflection spectra of the Si/Au hybrid nanostructures, including isolated and coupled Si nanopillars sitting on a thin Au film, were calculated by using the finite-difference time-domain (FDTD) technique. For regular arrays of Si nanopillars with different periods, the periodic boundary condition was applied in the lateral directions (x and y directions). For isolated Si nanopillars, a perfectly matched boundary condition was employed to terminate the simulation region. The refractive indices of Si and Au were taken from Aspnes and Studna[53] and Johnson and Christy.[54]

The three-dimensional far-field radiation patterns of the Si/Au hybrid nanostructures were also simulated by using the FDTD method. In this case, we first calculated the radiation pattern induced by dipole sources oriented along the x direction, which were placed at the center of Si nanopillars as excitation sources. A detector was placed 2000 nm above the Au film to detect the Poynting vector. Considering that the orientations of the dipole sources are random and only the radiations of the in-plane (X-Y plane) dipole sources are detected, the actual radiation patterns of a Si/Au hybrid nanostructure were obtained by the superposition of the radiation patterns induced by all in-plane dipole sources.

ASSOCIATED CONTENT

Supporting Information

The Supporting Information is available free of charge at https://pubs.acs.org/doi/10.1021/acsphotonics.2c00618.

Morphology characterization; determination of BIC; analysis of FW-BIC based on the temporal coupled-mode theory; reflection spectra calculated and measured; regular array of Si nanopillars excited by using p- and s-polarized white light; procedure for fabricating Si nanopillars; SEM images; experimental setup used for the optical characterization (PDF)

AUTHOR INFORMATION

Corresponding Author

Sheng Lan − *Guangdong Provincial Key Laboratory of Nanophotonic Functional Materials and Devices, School of Information and Optoelectronic Science and Engineering, South China Normal University, Guangzhou 510006, China;* orcid.org/0000-0002-7277-0042; Email: slan@scnu.edu.cn

Authors

Lidan Zhou − *Guangdong Provincial Key Laboratory of Nanophotonic Functional Materials and Devices, School of Information and Optoelectronic Science and Engineering, South China Normal University, Guangzhou 510006, China; State Key Laboratory of Optoelectronic Materials and Technologies, School of Electronics and Information Technology, Sun Yat-sen University, Guangzhou 51006, China;* orcid.org/0000-0003-3146-9082

Mingcheng Panmai − *Guangdong Provincial Key Laboratory of Nanophotonic Functional Materials and Devices, School of Information and Optoelectronic Science and Engineering, South China Normal University, Guangzhou 510006, China*

https://doi.org/10.1021/acsphotonics.2c00618
ACS Photonics 2022, 9, 2991−2999

Shulei Li − *Guangdong Provincial Key Laboratory of Nanophotonic Functional Materials and Devices, School of Information and Optoelectronic Science and Engineering, South China Normal University, Guangzhou 510006, China; School of Optoelectronic Engineering, Guangdong Polytechnic Normal University, Guangzhou 510665, China*

Yuheng Mao − *Guangdong Provincial Key Laboratory of Nanophotonic Functional Materials and Devices, School of Information and Optoelectronic Science and Engineering, South China Normal University, Guangzhou 510006, China*

Weichen He − *Guangdong Provincial Key Laboratory of Nanophotonic Functional Materials and Devices, School of Information and Optoelectronic Science and Engineering, South China Normal University, Guangzhou 510006, China;* orcid.org/0000-0003-0718-5063

Hongxin Huang − *Guangdong Provincial Key Laboratory of Nanophotonic Functional Materials and Devices, School of Information and Optoelectronic Science and Engineering, South China Normal University, Guangzhou 510006, China;* orcid.org/0000-0002-0398-5365

Complete contact information is available at: https://pubs.acs.org/10.1021/acsphotonics.2c00618

Author Contributions

#L.Z. and M.P. contributed equally to this work. L.Z. and M.P. carried out the numerical simulations; L.Z., M.P., S.L., Y.M., and W.H. fabricated the samples and performed the optical measurements; S.L., L.Z., and M.P. analyzed the data and wrote the manuscript; S.L. supervised the project. All the authors read and commented on the manuscript.

Funding

S.L. acknowledges the financial support from the National Natural Science Foundation of China (grant nos. 11874020 and 12174123).

Notes

The authors declare no competing financial interest.

REFERENCES

(1) Pavesi, L. Routes toward silicon-based lasers. *Mater. Today* **2005**, *8*, 18−25.
(2) Cullis, A. G.; Canham, L. T.; Calcott, P. D. J. The structural and luminescence properties of porous silicon. *J. Appl. Phys.* **1997**, *82*, 909−965.
(3) Stewart, M. P.; Buriak, J. M. Photopatterned Hydrosilylation on Porous Silicon. *Angew. Chem., Int. Ed.* **1998**, *37*, 3723−3257.
(4) Pavesi, L.; Dal Negro, L.; Mazzoleni, C.; Franzo, G.; Priolo, F. Optical gain in silicon nanocrystals. *Nature* **2000**, *408*, 440−444.
(5) de Boer, W. D. A. M.; Timmerman, D.; Dohnalova, K.; Yassievich, I. N.; Zhang, H.; Buma, W. J.; Gregorkiewicz, T. Red spectral shift and enhanced quantum efficiency in phonon-free photoluminescence from silicon nanocrystals. *Nat. Nanotechnol.* **2010**, *5*, 878−884.
(6) Martinez, A.; Blasco, J.; Sanchis, P.; Galan, J. V.; Garcia-Ruperez, J.; Jordana, E.; Gautier, P.; Lebour, Y.; Hernandez, S.; Guider, R.; Daldosso, N.; Garrido, B.; Fedeli, J. M.; Pavesi, L.; Marti, J.; Spano, R. Ultrafast all-optical switching in a silicon-nanocrystal-based silicon slot waveguide at telecom wavelengths. *Nano Lett.* **2010**, *10*, 1506−1511.
(7) Timmerman, D.; Valenta, J.; Dohnalová, K.; de Boer, W. D. A.; Gregorkiewicz, T. Step-like enhancement of luminescence quantum yield of silicon nanocrystals. *Nat. Nanotechnol.* **2011**, *6*, 710−713.
(8) Fadaly, E. M.; Dijkstra, A.; Suckert, J. R.; Ziss, D.; van Tilburg, M. A. J.; Mao, C.; Ren, Y.; van Lange, V. T.; Korzun, K.; Kolling, S.; Verheijen, M. A.; Busse, D.; Rodl, C.; Furthmuller, J.; Bechstedt, F.; Stangl, J.; Finley, J. J.; Botti, S.; Haverkort, J. E. M.; Bakkers, E. Direct-bandgap emission from hexagonal Ge and SiGe alloys. *Nature* **2020**, *580*, 205−209.
(9) Ródl, C.; Furthmüller, J.; Suckert, J. R.; Armuzza, V.; Bechstedt, F.; Botti, S. Accurate electronic and optical properties of hexagonal germanium for optoelectronic applications. *Phy. Rev. Mat.* **2019**, *3*, No. 034602.
(10) Wang, D.-C.; Zhang, C.; Zeng, P.; Zhou, W.-J.; Ma, L.; Wang, H.-T.; Zhou, Z.-Q.; Hu, F.; Zhang, S.-Y.; Lu, M.; Wu, X. An all-silicon laser based on silicon nanocrystals with high optical gains. *Sci. Bull.* **2018**, *63*, 75−77.
(11) Zeng, P.; Wang, F.; Zhang, Y.; Zhou, W.; Guo, Z.; Wu, X.; Lu, M.; Zhang, S. Edge-Emitting Silicon Nanocrystal Distributed Feedback Laser with Extremely Low Exciton Threshold. *ACS Photonics* **2021**, *8*, 1353−1363.
(12) Chen, S.; Li, W.; Wu, J.; Jiang, Q.; Tang, M.; Shutts, S.; Elliott, S. N.; Sobiesierski, A.; Seeds, A. J.; Ross, I.; Smowton, P. M.; Liu, H. Electrically pumped continuous-wave III−V quantum dot lasers on silicon. *Nat. Photonics* **2016**, *10*, 307−311.
(13) Staude, I.; Schilling, J. Metamaterial-inspired silicon nanophotonics. *Nat. Photonics* **2017**, *11*, 274−284.
(14) Wong, Z. J.; Xu, Y.-L.; Kim, J.; O'Brien, K.; Wang, Y.; Feng, L.; Zhang, X. Lasing and anti-lasing in a single cavity. *Nat. Photonics* **2016**, *10*, 796−801.
(15) Kristensen, P. T.; Hughes, S. Modes and Mode Volumes of Leaky Optical Cavities and Plasmonic Nanoresonators. *ACS Photonics* **2013**, *1*, 2−10.
(16) Liu, Z.; Xu, Y.; Lin, Y.; Xiang, J.; Feng, T.; Cao, Q.; Li, J.; Lan, S.; Liu, J. High-Q Quasi bound States in the Continuum for Nonlinear Metasurfaces. *Phys. Rev. Lett.* **2019**, *123*, No. 253901.
(17) Koshelev, K.; Kruk, S.; Melik-Gaykazyan, E.; Choi, J.-H.; Bogdanov, A.; Park, H.-G.; Kivshar, Y. Subwavelength dielectric resonators for nonlinear nanophotonics. *Science* **2020**, *367*, 288−292.
(18) Kuznetsov, A. I.; Miroshnichenko, A. E.; Brongersma, M. L.; Kivshar, Y. S.; Luk'yanchuk, B. Optically resonant dielectric nanostructures. *Science* **2016**, *354*, aag2472.
(19) Dong, Z.; Gorelik, S.; Paniagua-Dominguez, R.; Yik, J.; Ho, J.; Tjiptoharsono, F.; Lassalle, E.; Rezaei, S. D.; Neo, D. C. J.; Bai, P.; Kuznetsov, A. I.; Yang, J. K. W. Silicon Nanoantenna Mix Arrays for a Trifecta of Quantum Emitter Enhancements. *Nano Lett.* **2021**, *21*, 4853−4860.
(20) Ding, L.; Morits, D.; Bakker, R.; Li, S.; Eschimese, D.; Zhu, S.; Yu, Y. F.; Paniagua-Dominguez, R.; Kuznetsov, A. I. All-Optical Modulation in Chains of Silicon Nanoantennas. *ACS Photonics* **2020**, *7*, 1001−1008.
(21) Paniagua-Dominguez, R.; Ha, S. T.; Kuznetsov, A. I. Active and Tunable Nanophotonics With Dielectric Nanoantennas. *Proceedings of the IEEE* **2020**, *108*, 749−771.
(22) Kruk, S.; Kivshar, Y. Functional Meta-Optics and Nanophotonics Governed by Mie Resonances. *ACS Photonics* **2017**, *4*, 2638−2649.
(23) Kuznetsov, A. I.; Miroshnichenko, A. E.; Fu, Y. H.; Zhang, J.; Luk'yanchuk, B. Magnetic light. *Sci. Rep.* **2012**, *2*, 492.
(24) Xu, J.; Wu, Y.; Zhang, P.; Wu, Y.; Vallée, R. A. L.; Wu, S.; Liu, X. Resonant Scattering Manipulation of Dielectric Nanoparticles. *Adv. Opt. Mater.* **2021**, *9*, 2100112.
(25) Staude, I.; Pertsch, T.; Kivshar, Y. S. All-Dielectric Resonant Meta-Optics Lightens up. *ACS Photonics* **2019**, *6*, 802−814.
(26) Jahani, S.; Jacob, Z. All-dielectric metamaterials. *Nat. Nanotechnol.* **2016**, *11*, 23−36.
(27) Koshelev, K.; Kivshar, Y. Dielectric Resonant Metaphotonics. *ACS Photonics* **2021**, *8*, 102−112.
(28) Zhang, C.; Xu, Y.; Liu, J.; Li, J.; Xiang, J.; Li, H.; Li, J.; Dai, Q.; Lan, S.; Miroshnichenko, A. E. Lighting up silicon nanoparticles with Mie resonances. *Nat. Commun.* **2018**, *9*, 2964.
(29) Xiang, J.; Chen, J.; Dai, Q.; Tie, S.; Lan, S.; Miroshnichenko, A. E. Modifying Mie Resonances and Carrier Dynamics of Silicon Nanoparticles by Dense Electron-Hole Plasmas. *Phys. Rev. Applied* **2020**, *13*, No. 014003.

(30) Cho, C. H.; Aspetti, C. O.; Park, J.; Agarwal, R. Silicon coupled with plasmon nanocavity generates bright visible hot-luminescence. *Nat. Photonics* **2013**, *7*, 285−289.
(31) Xiang, J.; Panmai, M.; Bai, S.; Ren, Y.; Li, G. C.; Li, S.; Liu, J.; Li, J.; Zeng, M.; She, J.; Xu, Y.; Lan, S. Crystalline Silicon White Light Sources Driven by Optical Resonances. *Nano Lett.* **2021**, *21*, 2397−2405.
(32) Xifré-Pérez, E.; Shi, L.; Tuzer, U.; Fenollosa, R.; Ramiro-Manzano, F.; Quidant, R.; Meseguer, F. Mirror-Image-Induced Magnetic Modes. *ACS Nano* **2013**, *7*, 664−668.
(33) Yang, G.; Dev, S. U.; Allen, M. S.; Allen, J. W.; Harutyunyan, H. Optical Bound States in the Continuum Enabled by Magnetic Resonances Coupled to a Mirror. *Nano Lett.* **2022**, *22*, 2001−2008.
(34) Bulgakov, E. N.; Sadreev, A. F. Light trapping above the light cone in a one-dimensional array of dielectric spheres. *Phys. Rev. A* **2015**, *92*, No. 023816.
(35) Zhen, B.; Hsu, C. W.; Lu, L.; Stone, A. D.; Soljačić, M. Topological nature of optical bound states in the continuum. *Phys. Rev. Lett.* **2014**, *113*, No. 257401.
(36) Huang, C.; Zhang, C.; Xiao, S.; Wang, Y.; Fan, Y.; Liu, Y.; Zhang, N.; Qu, G.; Ji, H.; Han, J.; Ge, L.; Kivshar, Y.; Song, Q. Ultrafast control of vortex microlasers. *Science* **2020**, *367*, 1018−1021.
(37) Liu, M.; Choi, D. Y. Extreme Huygens' Metasurfaces Based on Quasi-Bound States in the Continuum. *Nano Lett.* **2018**, *18*, 8062−8069.
(38) Koshelev, K.; Bogdanov, A.; Kivshar, Y. Meta-optics and bound states in the continuum. *Sci. Bull.* **2019**, *64*, 836−842.
(39) Hsu, C. W.; Zhen, B.; Stone, A. D.; Joannopoulos, J. D.; Soljačić, M. Bound states in the continuum. *Nat. Rev. Mater.* **2016**, *1*, 16048.
(40) Liu, W.; Wang, B.; Zhang, Y.; Wang, J.; Zhao, M.; Guan, F.; Liu, X.; Shi, L.; Zi, J. Circularly Polarized States Spawning from Bound States in the Continuum. *Phys. Rev. Lett.* **2019**, *123*, No. 116104.
(41) Kodigala, A.; Lepetit, T.; Gu, Q.; Bahari, B.; Fainman, Y.; Kanté, B. Lasing action from photonic bound states in continuum. *Nature* **2017**, *541*, 196−199.
(42) Ha, S. T.; Fu, Y. H.; Emani, N. K.; Pan, Z.; Bakker, R. M.; Paniagua-Domínguez, R.; Kuznetsov, A. I. Directional lasing in resonant semiconductor nanoantenna arrays. *Nat. Nanotechnol.* **2018**, *13*, 1042−1047.
(43) Anthur, A. P.; Zhang, H.; Paniagua-Dominguez, R.; Kalashnikov, D. A.; Ha, S. T.; Mass, T. W. W.; Kuznetsov, A. I.; Krivitsky, L. Continuous Wave Second Harmonic Generation Enabled by Quasi-Bound-States in the Continuum on Gallium Phosphide Metasurfaces. *Nano Lett.* **2020**, *20*, 8745−8751.
(44) Xu, L.; Zangeneh Kamali, K.; Huang, L.; Rahmani, M.; Smirnov, A.; Camacho-Morales, R.; Ma, Y.; Zhang, G.; Woolley, M.; Neshev, D.; Miroshnichenko, A. E. Dynamic Nonlinear Image Tuning through Magnetic Dipole Quasi-BIC Ultrathin Resonators. *Adv. Sci. (Weinh)* **2019**, *6*, 1802119.
(45) Murai, S.; Abujetas, D. R.; Castellanos, G. W.; Sánchez-Gil, J. A.; Zhang, F.; Rivas, J. G. Bound States in the Continuum in the Visible Emerging from out-of-Plane Magnetic Dipoles. *ACS Photonics* **2020**, *7*, 2204−2210.
(46) Fang, C.; Yang, Q.; Yuan, Q.; Gan, X.; Zhao, J.; Shao, Y.; Liu, Y.; Han, G.; Hao, Y. High-Q resonances governed by the quasi-bound states in the continuum in all-dielectric metasurfaces. *Opto-Electron. Adv.* **2021**, *4*, 200030−200030.
(47) Dong, Z.; Jin, L.; Rezaei, S. D.; Wang, H.; Chen, Y.; Tjiptoharsono, F.; Ho, J.; Gorelik, S.; Ng, R. J. H.; Ruan, Q.; Qiu, C.-W.; Yang, J. K. W. Schrödinger's red pixel by quasi-bound-states in-the-continuum. *Sci. Adv.* **2022**, *8*, No. eabm4512.
(48) Liang, Y.; Koshelev, K.; Zhang, F.; Lin, H.; Lin, S.; Wu, J.; Jia, B.; Kivshar, Y. Bound States in the Continuum in Anisotropic Plasmonic Metasurfaces. *Nano Lett.* **2020**, *20*, 6351−6356.
(49) Xiang, J.; Xu, Y.; Chen, J.-D.; Lan, S. Tailoring the spatial localization of bound state in the continuum in plasmonic-dielectric hybrid system. *NANO* **2020**, *9*, 133−142.
(50) Panmai, M.; Xiang, J.; Li, S.; He, X.; Ren, Y.; Zeng, M.; She, J.; Li, J.; Lan, S. Highly efficient nonlinear optical emission from a subwavelength crystalline silicon cuboid mediated by supercavity mode. *Nat. Commun.* **2022**, *13*, 2749.
(51) Suh, W.; Wang, Z.; Fan, S. Temporal coupled-mode theory and the presence of non-orthogonal modes in lossless multimode cavities. *IEEE J. Quantum Electron.* **2004**, *40*, 1511−1518.
(52) Kang, M.; Zhang, S.; Xiao, M.; Xu, H. Merging Bound States in the Continuum at Off-High Symmetry Points. *Phys. Rev. Lett.* **2021**, *126*, No. 117402.
(53) Aspnes, D. E.; Studna, A. A. Dielectric functions and optical parameters of Si, Ge, GaP, GaAs, GaSb, InP, InAs, and InSb from 1.5 to 6.0 eV. *Phys. Rev. B* **1983**, *27*, 985−1009.
(54) Johnson, P. B.; Christy, R. W. Optical Constants of the Noble Metals. *Phys. Rev. B* **1972**, *6*, 4370−4379.

https://doi.org/10.1021/acsphotonics.2c00618
ACS Photonics 2022, 9, 2991−2999